Bioorganic Chemistry 90 (2019) 103037

Contents lists available at ScienceDirect

Bioorganic Chemistry

journal homepage: www.elsevier.com/locate/bioorg

Probing the binding mechanism of capecitabine to human serum albumin using spectrometric methods, molecular modeling, and chemometrics approach

S. Fatemeh Mousavi*, Mohammad Hossein Fatemi

Chemometrics Laboratory, Faculty of Chemistry, University of Mazandaran, Babolsar, Iran

ARTICLE INFO

Keywords:
Capecitabine
Human serum albumin (HAS)
Fluorescence spectroscopy
MCR-ALS
Molecular dynamics simulation
Molecular docking

ABSTRACT

Capecitabine as a prodrug of 5-Fluorouracil plays an important role in the treatment of breast and gastrointestinal cancers. Herein, in view of the importance of this drug in chemotherapy, interaction mechanism between Capecitabine (CAP) and human serum albumin (HSA) as a major transport protein in the blood circulatory system has been investigated by using a combination of spectroscopic and molecular modeling methods. The fluorescence spectroscopic results revealed that capecitabine could effectively quench the intrinsic fluorescence of HSA through a static quenching mechanism. Evaluation of the thermodynamic parameters suggested that the binding process was spontaneous while hydrogen bonds and van der Waals forces played a major role in this interaction. The value of the binding constant ($K_b = 1.820 \times 10^4$) suggested a moderate binding affinity between CAP and HSA which implies its easy diffusion from the circulatory system to the target tissue. The efficiency of energy transfer and the binding distance between the donor (HSA) and acceptor (CAP) were determined according to forster theory of nonradiation energy transfer as 0.410 and 4.135 nm, respectively. Furthermore, UV–Vis spectroscopic results confirmed that the interaction was occurred between HSA and CAP and caused conformational and micro-environmental changes of HSA during the interaction. Multivariate curve resolution-alternating least square (MCR-ALS) methodology as an efficient chemometric tool was used to separate the overlapped spectra of the species. The MCR-ALS result was exploited to estimate the stoichiometry of interaction and to provide concentration and structural information about HSA-CAP interactions. Molecular docking studies suggested that CAP binds mainly to the subdomain IIA of HSA, which were compatible with those obtained by experimental data. Finally, molecular dynamics simulation (MD) was performed on the best docked complex by considering the permanence and flexibility of HSA-CAP complex in the binding site. MD result showed that CAP could steadily bind to HSA in the site I based on the formation of hydrogen bond and π-π stacking interaction in addition to hydrophobic force.

1. Introduction

5-Fluorouracil (5-FU) is known as a key anticancer drug that has played an important role in the treatment of breast and gastrointestinal cancers, either in monotherapy or combination therapy with various cytotoxic drugs [1]. 5-FU is an analogue of pyrimidine uracil with a fluorine atom at the C-5 position in place of hydrogen [2]. After parental administration of 5-FU, it quickly enters the cell by using the same transport mechanism as uracil [3] and is converted intracellularly to active metabolites [4]. To optimize the efficacy of 5-FU, it is administered parentally, but this treatment has side effects such as gastrointestinal toxicity and myelosuppression. This quality of 5-FU administration is accompanied by the inconvenience and high treatment cost, including those for administration and toxicity related hospitalization like other cytotoxic drug administration. Capecitabine (CAP, Fig. S1) is an orally administered prodrug of 5-FU, which is considered as a convenient option for self-administration that mostly suits for patients who want to maintain their independence [5]. It is readily passed intact through the intestinal mucosa and is ultimately converted to 5-FU especially in tumor cells. This selectivity is achieved by the thymidine phosphorylase enzyme (TP), as the final conversion of capecitabine to 5-FU, which is more active in tumor cells compared to normal tissues [6].

In drug discovery, interactions between drug and human serum albumin (HSA), as a major transport protein in the blood circulatory system, play an important role in pharmacokinetics and

* Corresponding author.
E-mail addresses: fatemehmehrasa85@yahoo.com (S.F. Mousavi), mhfatemi@umz.ac.ir (M.H. Fatemi).

https://doi.org/10.1016/j.bioorg.2019.103037
Received 19 November 2018; Received in revised form 27 May 2019; Accepted 3 June 2019
Available online 08 June 2019

pharmacodynamics behavior of the drugs [7]. Solubility, half-life, metabolism, distribution and excretion of biological active compound (drugs or natural products) are associated with their affinity toward HSA [8,9]. HSA is a single chain, globular protein made up of 585 amino acid residues, and 17 disulfide bridges in a heart shape molecule. Crystallographic data show that HSA contains three homologous α-helix domains (I-III) that each one is composed of two subdomains (A and B) [10]. HSA molecule has two specific ligand binding sites called Sudlow's site I and site II that are located in hydrophobic cavities in subdomains IIA and IIIA, respectively [11]. These multiple binding sites increase the exceptional ability of HSA to binding, transporting and delivering a wide range of physiological functions such as fatty acids, hormones, amino acids, toxic metabolites, drugs and metals to their target organs. Furthermore, binding of biological active compounds to the HSA may also have an influence on the structure and function of this protein [12]. Therefore, studying the interaction between drugs and proteins at the molecular level is important not only to understand relationship between chemical structure and pharmacological activity, but also to investigate the effect of drugs on the structure and function of the protein in the body. There are many techniques to study the interaction mechanism of drugs with serum albumin, such as; spectroscopy (FT-IR, CD, fluorescence, synchronous fluorescence, UV–Vis absorption and 3D fluorescence spectra) [13–16], electrochemistry [17], High-performance liquid chromatography (HPLC) [18], Nuclear magnetic resonance (NMR) spectroscopy [19], isothermal titration calorimetry (ITC) [20], scanning electron microscopy (SEM) and transmission electron microscopy (TEM) analyses [21] as well as computational methods like molecular docking and molecular dynamic (MD) simulation [22]. However, in the multicomponent reaction system reported above, it is difficult to extract significant quantitative information from the composite spectral profile by the common methods of data interpretation. So, in order to solve this problem, chemometrics methods such as multivariate curve resolution-alternating least squares (MCR-ALS) technique are applied [23]. This method can provide further information about the complex formation, the concentration profiles and pure spectra of each species.

Investigation on binding properties between capecitabine and human serum albumin is clearly important since it can provide useful information for clinical and pharmaceutical application of these biologically important molecules. Several pharmacokinetic studies have been performed on CAP, but amongst them, just one study was performed to investigate the interaction of CAP with HSA by using ^{19}F NMR spectroscopy [19]. This report showed that capecitabine was effectively bound to HSA in subdomain IIA (Sudlow's site I) and different degrees of microenvironment and conformational change was happened in HSA but its overall structure was remained unchanged in this interaction. In the present work, multispectroscopic techniques have been used to study the quenching mechanism, thermodynamic parameters as well as binding parameters of HSA-CAP complexes. Moreover, MCR-ALS as a soft modeling method was applied to extract information from overlapping responses of the reaction participants from spectroscopic data so that it can help to understand further the complex kinetic processes and elucidate the contribution of any species involved in the interaction, and also their concentration profiles and spectra. In the second step, molecular modeling studies have been used to improve the understanding of the interaction of CAP with HSA at the molecular level. Docking study as a fast and inexpensive method has been performed to characterize the CAP binding site, important residue included, and main position of the ligand. Science in the docking studies, flexibility of the protein has not been taken into consideration, therefore, MD simulation have been carried out to consider the mobility of both protein and ligand during the binding. The present study is expected to make complement the prior studies and provide valuable information regarding the biological effects of CAP at the molecular level.

2. Experimental

2.1. Chemicals and solutions

Commercially prepared human serum albumin (HSA, purity > 99.0%) was purchased from Sigma-Aldrich (St. Louis, MO, USA). CAP was procured from Baran Co. (Tehran, Iran). All other reagents were analytical grade, and doubly distilled water was used in all experiments. A stock solution of HSA (300 μM) was prepared in phosphate buffer (0.05 mol L^{-1}, pH = 7.4) and were kept in the refrigerator at dark place. Stock solution of CAP (0.6 mM) was prepared in water. Experimental solutions of HSA and CAP were prepared by appropriate dilution of their stock solutions.

2.2. Instruments and softwares

Fluorescence measurements were performed on a PC based spectrofluorometer (JASCO Japan FP-8300) equipped with a Xenon lamp and 1.0 cm quartz cell. The UV–Vis absorption spectrum was recorded at room temperature on a SQ4802 UV–Vis Diode-Array spectrophotometer equipped with 1.0 cm quartz cells. The pH values were measured by using Metrohm, model 691, pH/mV meter. The chemical structure of the CAP was sketched in Gauss View 5 and optimization steps were carried out by DFT method at the B3LYP/6-311 + + G^{**} levels of theory in Gaussian 09 W molecular modeling package [24]. The X-ray crystal structure of HSA was retrieved from the protein data bank (PDB ID code: 2BXD) [25]. Autodock 4.2 program was employed to generate a docked conformation of CAP with HSA [26]. MD simulations were carried out by the NAMD 2.9 program [27] by using the CHARMM 22 force field. MCR-ALS analyses were performed by using the MCR-ALS 2.0 MATLAB toolbox [28].

2.3. Spectroscopic studies

2.3.1. Fluorescence quenching measurements

Fluorescence titrations were carried out using a fixed concentration of HSA (5.0×10^{-3} mol L^{-1}) in the presence of different amounts of CAP (0.0–30.0 $\times 10^{-6}$ mol L^{-1}; interval concentration: 1.5×10^{-6} mol L^{-1}). The excitation wavelength was set to 280 nm, and the emission spectra were recorded at wavelengths from 290 to 550 nm. Prior to fluorescence measurements, samples were thermally equilibrated at 298 K, 305 K, and 310 K for about 20 min. The titrations are done manually using the 10 μL microsyringe. The excitation and emission slit widths were set at 5 nm.

2.3.2. Development of the expanded data matrix for MCR–ALS

Fluorescence and UV–Vis spectroscopic experiments were carried out in phosphate buffer (0.01 mol L^{-1}) of pH 7.4 at 298 K. Two separate experiments were performed based on the mole-ratio method. In experiment 1, the concentration of HSA was kept constant (5.0×10^{-3} mol L^{-1}) while the CAP concentration is increased in the range of 0.0–30.0 $\times 10^{-6}$ mol L^{-1} with an interval of 1.5×10^{-6} mol L^{-1}. On the other hand, in experiment 2 the concentration of the CAP was fixed at 7.2×10^{-6} mol L^{-1} while different values of HSA (0.0–7.2 $\times 10^{-6}$ mol L^{-1} with an interval of 3.6×10^{-7} mol L^{-1}) were added to this solution. In both cases after addition of titrant in each step, the solution was stirred and allowed to stand for 5 min, then the fluorescence (290–550 nm with a wavelength interval of 1 nm) and UV–Vis (245–400 nm with an interval of 1 nm) spectra of this solution were recorded. At the end, four data matrices, D_F^{HSA}, D_{UV}^{HSA} and D_F^{CAP}, D_{UV}^{CAP} were obtained from these measurements. D_F^{HSA} and D_{UV}^{HSA} refer to fluorescence and absorption spectra of experiment 1 while D_F^{CAP} and D_{UV}^{CAP} are the fluorescence and absorption spectra of experiment 2. These four data matrices were combined and an expanded data matrix, D, was created to satisfy the full rank conditions.

2.4. Chemometrics methods

MCR-ALS is a well-known multivariate self-modeling curve resolution method which is applicable to resolve the multicomponent mixtures into pure contributions of constituents only from the information obtained from an original two-way data matrix [28,29]. This method is based on the bilinear decomposition of the experimental data set, D, into the product of two matrices, C and S^T that contains pure components profiles in a mixture system. The bilinear model is expressed in the following way:

$$D = CS^T + E \quad (1)$$

where D is the matrix of experimental data with dimension of M (spectral object) × N (wavelengths), C (M × P) is the matrix of concentration profile of P species existing in the given measurement profiles, S^T (P × N) is the pure spectra of P species, and E is the matrix of residuals with the data variance unexplained by the model. During the ALS optimization, different types of constraint (such as non-negativity and unimodality) are applied to C and S^T in each iteration in order to provide physically meaningful and chemically interpretable solutions, and facilitate the finding of pure or most representative contributions to the data matrix using real variables [30]. Also, the use of multiset structure along with soft modelling constraints greatly helps to make the solution more robust [31,32]. In this way, when different data matrices are augmented and simultaneously analyzed by MCR-ALS method, the number of possible solutions of Eq. (1) is substantially reduced and, hopefully, converged to a unique solution. In the present study, the augmented data matrix of the two-way fluorescence and UV–Vis spectral data (D) is built up by placing the individual data matrices corresponding to the two experiments series side by side [33,34]. The related bilinear model for MCR-ALS analysis is given by Eq. (2):

$$[D_F \;\; D_{UV}] = C\,[S_F^T S_{UV}^T] + [E_F E_{UV}] \quad (2)$$

If D_F and D_{uv} were the data matrices obtained with the two spectroscopic techniques, there would be a single concentration profile matrix, C, and two row-wise augmented spectral matrix of measured spectra, S_{UV}^T and S_F^T, which contain the pure signals of the spectroscopic techniques used to obtain D_F, and D_{uv} matrices, respectively.

In order to assess the quality of the obtained MCR-ALS model, lack of fit (LOF) as a statistical parameter is calculated by using Eq. (3) which describes the difference between the original data set, D, and the approximation made for it by the CS_T product of the extended MCR–ALS analysis.

$$\mathrm{LOF}(\%) = 100 \times \sqrt{\frac{\sum_{ij}(d_{ij}^* - d_{ij})^2}{\sum d_{ij}^2}} \quad (3)$$

In the above equation, d_{ij} is an element of the experimental matrix D and d_{ij}^* is the analogous element of the reproduced data matrix (CS^T) obtained by the MCR-ALS model [35].

2.5. Molecular docking studies

Molecular docking studies were performed to probe the binding site in HSA and to predict the conceivable orientation of the molecule during the ligand-protein interaction. Herein, the AutoDock4.2 software package [26] was used to perform the molecular docking, along with sampling based on the empirical free energy function and the Lamarckian genetic algorithm (LGA) method. Protein coordinates were extracted from the crystal structure of HSA-inhibitor complexes with the code 2BXD in protein data bank [25].Some residues in the loop regions were not solved in the crystal structure, therefore, the missing residues were added by using the Modeler 9.19 software [36]. During the preparation of the protein input file, the Gasteiger charges were assigned to the receptor protein and the water molecules were removed, then, polar hydrogen atoms were added in AutoDock Tools environment. In docking routine, the protein was considered as a rigid body during the docking, but all torsion bonds in inhibitors were set free and the docking software was allowed to rotate all rotatable bonds of inhibitors to achieve the best and optimized conformer of the inhibitors within the active site of protein. In order to justify the location of ligand in the ligand-protein complex, a grid map was defined with a grid point spacing of 0.375 Å and 60 × 60 × 60 points, which included not only the binding site of the HSA but also the significant regions of the surrounding surface. The amount of independent docking runs carried out for each docking simulation was set to 100 and other parameters were maintained at the default settings. Cluster analysis (root mean square tolerance equal to 0.5 Å) was then performed on the docked results. The pose with the lowest binding energy on the cluster was considered for future analysis and as the initial structure for the molecular dynamics step.

2.6. Molecular dynamics simulations

In order to investigate the in-vivo stability of the docked complex, the MD simulations were performed in the presence of an explicit solvent by using NAMD software. The MD simulations were carried out by using NAMD 2.9 program [27] and applying the CHARMM 22 force field. The topology and force field parameters for the CAP were generated by using Swissparam webserver [37]. Pure HSA and HSA-CAP complex were solvated by simple point charge water molecule in the cubic box by using periodic boundary condition [38]. To avoid the direct interaction of the HSA complex with its own periodic image, the distances between complex and the box wall was kept at 12 Å. The solvated system was neutralized by adding Na^+ counter ions in the simulation. Initially, energy minimization of system was carried out to relieve unfavorable interactions by using 1000 steps of the steepest descent algorithm and subsequently 1000 steps of the conjugate gradient algorithm. Finally, the full system was subjected to 15 ns MD in an isothermal isobaric ensemble (NPT) at temperature of 310 K under 1 bar pressure. The temperature and pressure were kept constant by using Langevin dynamics and Nose-Hoover-Langevin piston, respectively. Lennard Jones interactions were calculated within a cut-off distance of 13.0 Å, and Particle Mesh Ewald (PME) was employed to deal with the long-range electrostatic interactions [39]. A time step of 2.0 fs was used for the overall simulations, and data were collected every 1 ps.

3. Results and discussion

3.1. Fluorescence and UV–Vis spectroscopy

Fluorescence spectroscopy has been extensively used to study the interaction between small molecules and protein due to its exceptional selectivity, sensitivity, convenience, and abundance of theoretical foundation [40]. This technique can provide useful information about the binding mechanism of the ligand to protein, such as; quenching mechanism, binding site, binding constant, and the interaction distances [41]. Intrinsic fluorescence emission of HSA is mainly derived from the tryptophan (Trp), tyrosine (Tyr) and phenylalanine (Phe) residues. However, the main contribution to the intrinsic fluorescence of the HSA comes from the tryptophan residues. The fluorescence of Trp residues is extremely sensitive to its environment. Fig. 1A and C display the fluorescence emission spectra obtained from experiment 1 and 2, respectively (see Section 2.3.2). As can be seen in Fig. 1A, the fluorescence intensity of HSA was gradually decreased with increasing concentration of CAP at fixed concentration of HSA. Additionally, a new intensive peak appeared at 387 nm which is the wavelength corresponding to the emission peak of CAP on its addition. Moreover, quenching of HSA was associated with a slight shift toward longer wavelengths which showed that HSA had interaction with HSA and

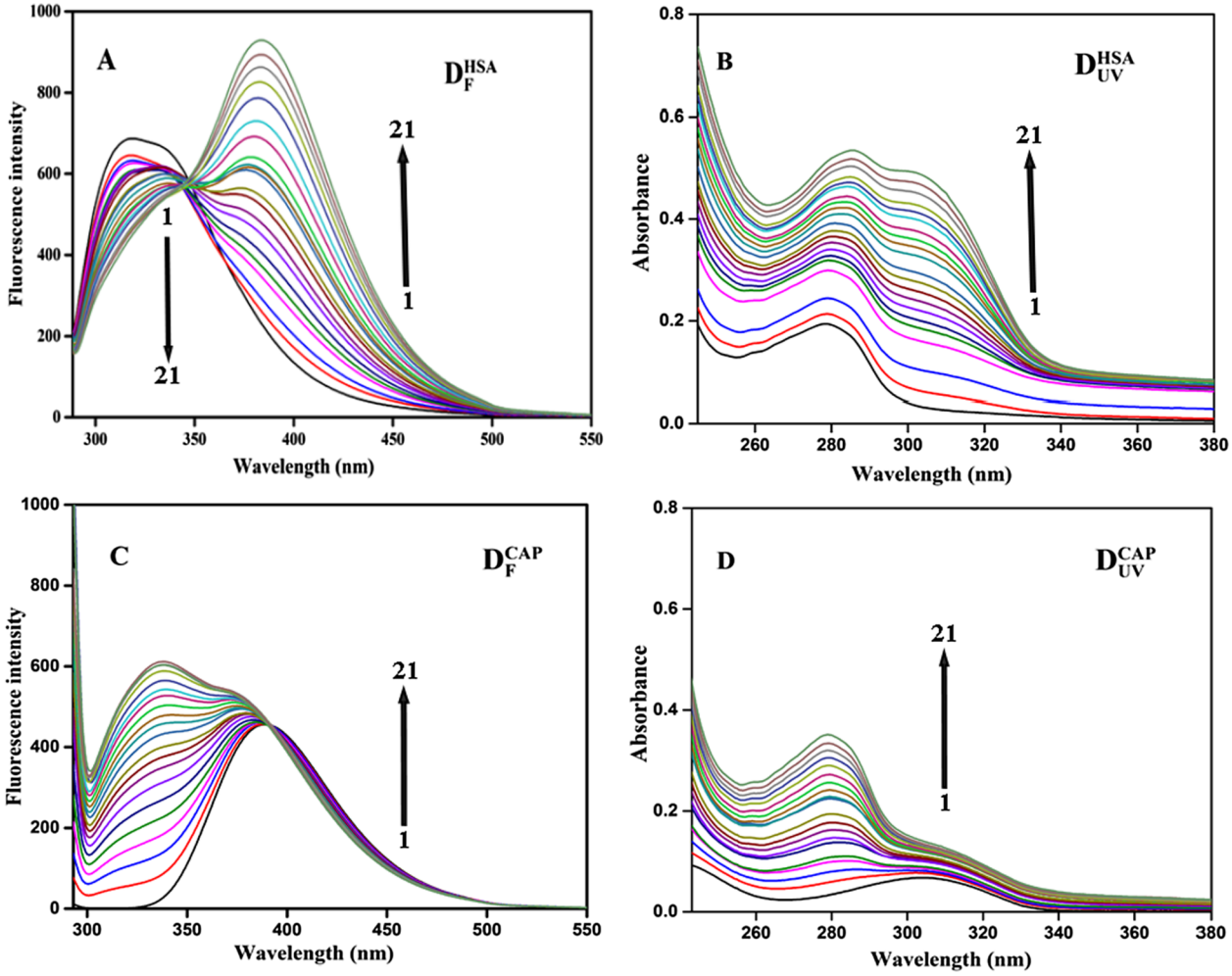

Fig. 1. Fluorescence emission and UV–Vis absorption spectra obtained from different experiments. Experiment 1: (A) fluorescence (D_F^{HSA}) and (B) UV–Vis (D_{UV}^{HSA}); $C_{HSA} = 5.0 \times 10^{-3}$ mol L^{-1}, $C_{CAP} = 0.0–30.0 \times 10^{-6}$ mol L^{-1}. Experiment 2: (C) fluorescence (D_F^{CAP}) and (D) UV–Vis (D_{UV}^{CAP}); $C_{CAP} = 7.2 \times 10^{-6}$ mol L^{-1}, $C_{HSA} = 0.0–7.2 \times 10^{-6}$ mol L^{-1}.

HSA-CAP complex is formed. Additionally, the microenvironment around the fluorophore (Trp_{214}) in the protein solution has been changed. The fluorescence spectra of CAP in the presence of different concentrations of HSA (Fig. 1C) showed that CAP fluorescence intensity was initially increased slightly and then increased more strongly with a distinct blue shift from 387 nm to 375 nm. Simultaneously, a new HSA fluorescence peak has been appeared at 338 nm.

UV–Vis absorption spectroscopy can be used as a simple and intuitive approach to explore the structural changes of protein and often can confirm the formation of a molecular complex [42]. Fig. 1B and D show the UV–Vis absorption spectra of the experiments 1 and 2, respectively. Absorption spectral of HSA at different concentrations of CAP (Fig. 1B) showed that the intensity of absorption peak for HSA at about 280 nm was increased continuously by addition of CAP. Furthermore, a distinct red shift (from 280 to 286) was observed at the maximum absorption wavelength which suggests that the fluorophore of HSA was placed in a more hydrophilic environment after addition of CAP. These results indicate the formation of HSA-CAP complex and conformational changes of HSA during the interaction. Moreover, a new absorption peak was appeared at around 305 nm which is related to CAP molecule. On the other hand, as shown in Fig. 1D, the absorption intensities of CAP were increased with increasing the concentration of HSA and a new peak was appeared at 280 nm. For further investigation and to obtain more information about the formation of HSA-CAP complex, these data were resolved by using MCR-ALS which is described in the next parts.

3.2. Quenching studies

The fluorescence quenching may be results of various processes such as excited-state reactions, molecular collision, molecular rearrangements, ground-state complex formation and energy transformation [43]. The mechanisms of these processes are frequently categorized into dynamic quenching and static quenching which can be distinguished with their different dependence on temperature, viscosity, and excited state lifetime. Static quenching is usually associated with complex formation between the fluorophore (protein) and the quencher which is decreased by increasing the temperature. On the contrary, dynamic quenching depends on the diffusion of species and since the increase in temperature results in faster diffusion of quencher, the quenching constants are expected to be increased with increasing temperature. To explore the quenching mechanism involved in the CAP-HSA system, the fluorescence quenching data at different temperatures was analyzed using the Stern–Volmer equation [44]:

$$\frac{F_0}{F} = 1 + K_{SV}[CAP] = 1 + K_q \tau_0 [CAP] \quad (4)$$

where F_0 and F are the fluorescence intensities before and after addition of CAP, respectively. K_{SV} is the Stern–Volmer quenching constant in L mol^{-1}, [CAP] is the concentration of CAP, Kq is the bimolecular

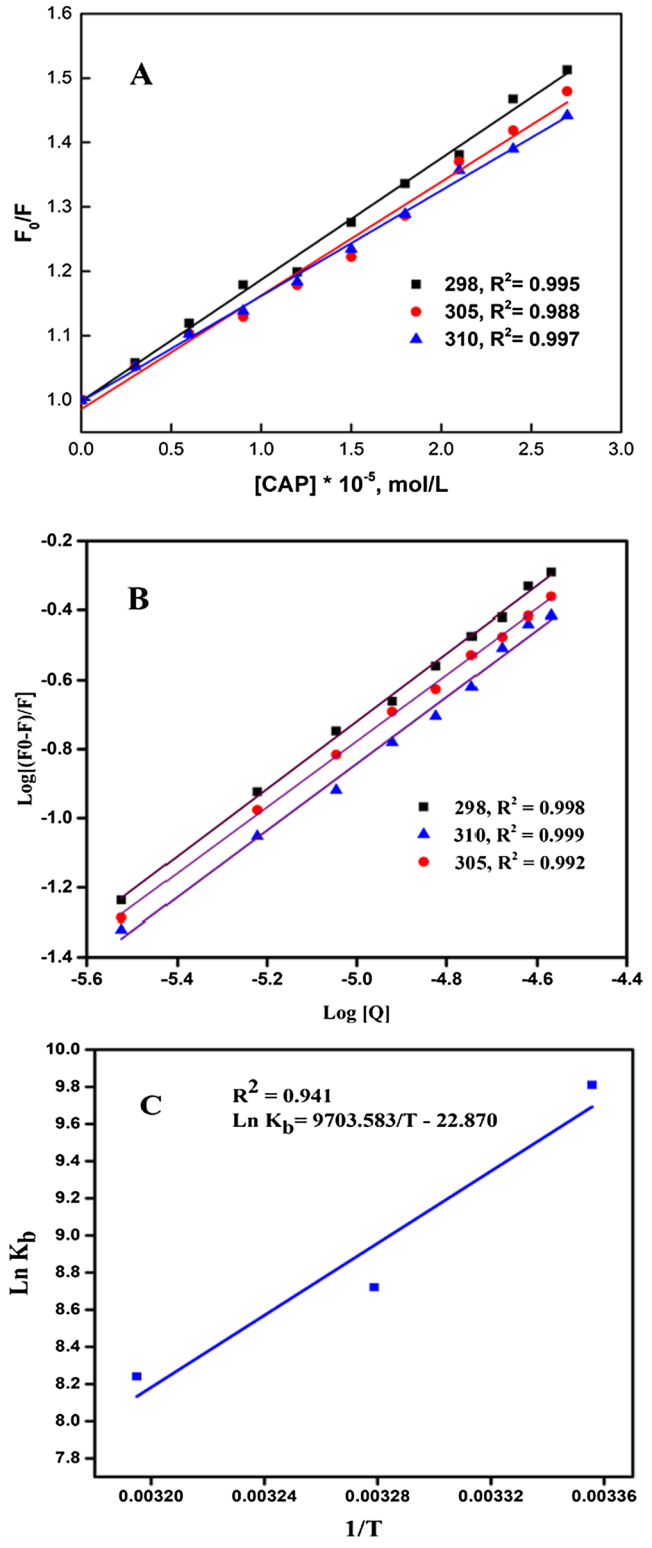

Fig. 2. (A) Stern-Volmer plots for the quenching of HSA by CAP at different temperatures. (B) Plot of log [(F_0-F)/F] versus log [Q] for the HSA–CAP system at three different temperatures. (C) van't Hoff plot of the HSA-CAP system.

quenching rate constant, and τ_0 (10^{-8} s) is the average lifetime of the HSA without CAP as a quencher and is generally equal to 10^{-8} s [45]. The Stern–Volmer plots for quenching of fluorescence emission of HSA in the presence of CAP at three different temperatures are shown in Fig. 2A. The obtained values of K_{SV} and K_q are listed in Table 1. As shown in this table, the K_{SV} values of the systems inversely correlate with the temperature, furthermore, corresponding k_q values are much greater than the maximum scatter collision quenching constant of the biopolymers ($K_q = 2.0 \times 10^{10}$ L mol^{-1} s^{-1}) [46], indicating that the quenching is caused by formation of a complex between HSA and CAP, rather than by a dynamic collision [47].

3.3. Binding parameters

In static quenching, it is assumed that several binding sites (n) are available on the HSA that the drug can bind independently to these sites. The binding constant and n involved in the CAP-HSA system can be determined according to the modified Stern–Volmer equation as follows [48]:

$$\log\frac{F_0 - F}{F} = \log K_b + n\log[CAP] \quad (5)$$

The values of K_b and n were obtained from the intercept and slope of the plot of log [(F_0 − F)/F] versus log [CAP] at three different temperatures (Fig. 2B), respectively and are listed in Table 1. As it is seen in this table, the values of n are approximately equal to 1 at different temperatures, suggesting that there is one high affinity binding site in the HSA for CAP. The binding constant (K_b) between drug and HSA is the main factor in its accessibility to diffuse from the circulatory system to the target, K_b values indicate the drug is bound to protein which will have diminished concentration of free fraction of drug in plasma while weakly bound drugs have faster clearances and shorter stay in the body [49]. The value of binding constant ($K_b = 1.820 \times 10^4$) for HSA-CAP system, suggest a moderate binding affinity when compared to protein-ligand complexes with higher binding constants (10^6–10^8) [50–52]. So the moderate binding in the present case indicates that CAP cannot be tightly stored and carried by HSA in the body and eventually, it would be transferred and released in the target tissue [53]. In addition, it was clear that the value of K_b was declined with increasing the temperature. This was coincided with the changes in the K_{SV}, and suggested that the quenching mechanism should belong to static quenching [54].

3.4. Thermodynamic parameters analysis

Essentially, there are four main types of non-covalent interactions including van der Waals forces, electrostatic, hydrophobic and H-bonds, which exist in ligand binding to macromolecules [55]. The thermodynamic parameters such as enthalpy change (ΔH^0), entropy change (ΔS^0) and free energy change (ΔG^0) of the reaction, play an important role to confirm the non-covalent acting forces. Ross and Subramanian have reported that the signs and magnitudes of the thermodynamic parameters (ΔH^0 and ΔS^0) can provide a strong evidence to confirm the binding forces [56]. That is, if $\Delta H^0 > 0$, $\Delta S^0 > 0$, the main force would be hydrophobic interaction, while van der Waals and hydrogen-bonding interactions play major roles in the reaction, if $\Delta H^0 < 0$, $\Delta S^0 < 0$ [57]. Since in the studied temperature range, the temperature effect was very small, the enthalpy change (ΔH^0) of a system can be regarded as a constant. Under these conditions, the values of the enthalpy (ΔH^0) and entropy changes (ΔS^0) for the HSA-CAP system can be calculated from the slope and intercept of the linear van't Hoff plot (Fig. 2C) of ln K versus 1/T according to following equation [58]:

$$Ln\ K_b = -\frac{\Delta H^0}{RT} + \frac{\Delta S^0}{R} \quad (6)$$

where K_b is the binding constant at the corresponding temperature (T), and R (J mol1 K1) is the gas constant.

The value of free energy change (ΔG) is estimated from the following relationship:

$$\Delta G^0 = \Delta H^0 - T\Delta S^0 \quad (7)$$

The obtained values of ΔH^0, ΔS^0, and ΔG^0 for HSA-CAP interaction are summarized in Table 1. The negative sign for free energy (ΔG^0) in

Table 1
Binding and thermodynamic parameters of the CAP–HSA system, studied at different temperatures.

	T (K)	K_{SV} ($L\,M^{-1}$)	K_q	K_b ($L\,M^{-1}$)	n	ΔH^0 ($kJ\,mol^{-1}$)	ΔS^0 ($J\,mol^{-1}$) K^{-1}	ΔG^0 ($kJ\,mol^{-1}$)
CAP	298	$1.971 \pm 0.004 \times 10^4$	$1.971 \pm 0.004 \times 10^{12}$	$1.820 \pm 0.084 \times 10^4$	0.998	−80.475	−189	−24.301
	305	$1.908 \pm 0.006 \times 10^4$	$1.908 \pm 0.006 \times 10^{12}$	$6.109 \pm 0.155 \times 10^3$	0.899			−24.882
	310	$1.606 \pm 0.003 \times 10^4$	$1.606 \pm 0.003 \times 10^{12}$	$3.801 \pm 0.059 \times 10^3$	0.865			−25.283

Table 1 means that the binding process is spontaneous under physiological conditions. The negative enthalpy (ΔH^0) and entropy (ΔS^0) values of the interaction of CAP and HSA indicate that the binding is mainly enthalpy driven, whereas the entropy is unfavorable to it, where, hydrogen bonds and van der Waals forces played a major role in the reaction. Regarding the structure of the CAP, which contains two hydroxyls and one amino group, it was expected that the hydrogen bond can be formed between these functional groups and HSA.

3.5. Interpretation of the MCR-ALS results

It is difficult to distinguish the formation of a complex in the binding reaction systems and deduce the changes in concentration of reaction components during the titration process only based on the fluorescence and UV–vis spectra (Fig. 1A–D), due to the high spectral overlap which is observed for each species. Therefore, multivariate analysis of the recorded experimental data was performed by MCR-ALS as a powerful chemometric tool to extract more useful information regarding the formation of any HSA$[CAP]_m$ complex, and also about the relative concentrations of the various reactant and product species. Therefore, individual data matrices obtained from UV–Vis and fluorescence measurement were combined into two row-wise augmented data matrices $[D_F^{HSA} S_{UV}^{HSA}]$,$[D_F^{CAP} D_{UV}^{CAP}]$, respectively, as previously explained, and then these augmented matrices were submitted for simultaneous resolution by MCR-ALS. Before starting the resolution, the number of contributions to the augmented matrix was determined by using singular value decomposition (SVD) (Table S1). The results indicated that four significant factors can account for the spectral features. One guess is that two of these four components can be related to free CAP and free HSA, while the rest of them can belong to the complex species. Taking into account that MCR–ALS needs information as real as possible to start the resolution, the concentration profiles of the species existing in the binding procedure were estimated by the use of the Evolving Factor Analysis (EFA). Then, resolution of augmented data matrix was obtained by using MCR-ALS and applying the constraint of non-negativity during the repetitive process for both concentration and spectral profiles and also the total concentrations of HSA and CAP were known in the systems, and they were used as a closure constraint for the concentration profiles. As previously mentioned, the quality and reliability of the MCR-ALS solution may be assessed using the percent of lack of fit (LOF) and explained variance (R^2) parameters that allow assessing the dissimilarity among the input data (***D***) and the data reproduced from the product (***CS***T) obtained by MCR-ALS. In this study, the best LOF and R^2 values for the experiments at constant concentration of HSA and CAP were obtained to be 0.396, 99.998% and 0.884%, 99.992%, respectively, which implied that almost all variability of the experimental data has been modelled.

The results obtained from MCR-ALS are shown in Fig. 3A-D. Fig. 3A and B represent the extracted concentration profiles of the species involved in the experiments. Fig. 3A shows that when CAP is added to HSA, concentration of HSA is decreased and two new complex species are formed. As can be seen in this figure, concentration of the first complex species is increased and reached a maximum at [CAP]/[HSA] = 1 which is a 1:1 HSA-CAP complex specie. On the other hand, concentration of the second species was increased sharply and reached a maximum at the ratio of [CAP]/[HSA] = 3. Therefore, it may be concluded that this specie is a 1:3 HSA-CAP complex specie. Also, it can be observed from this figure that after the point of [CAP]/[HSA] = 3, CAP is released which suggests that the formation of complex between HSA and CAP is finished and also only two complex species were formed upon the addition of CAP to HSA. In order to judgment about the stoichiometry of complex species and make a reasonable decision about these species, the results of Fig. 3B should also be considered. This figure showed that the concentration of second species was increased and reached a maximum at [HSA]/[CAP] = 0.33 which confirms the formation of 1:3 HSA-CAP complex. Thus, as can be seen, concentration of first species was increased and reached a maximum at [HSA]/[CAP] = 1, which confirms the formation of 1:1 HSA-CAP complex. Fig. 3C and D show the pure fluorescence and UV–Vis spectral profiles resolved by MCR-ALS for different species which provide new qualitative information about the nature of the species involved in each technique. As can be seen, the pure fluorescence and absorption spectra of four components (HSA, CAP, and two HSA-CAP complex species, solid line) were extracted and the resolved spectra of CAP and HSA agreed well with the measured spectra (dashed lines). This agreement between the theoretical and experimental data is a strong evidence for the high quality of the fitting process and indicates that the concentration profiles were correctly resolved. It's important to note that the fluorescence and UV–Vis spectra of the HSA$[CAP]_m$ complex, which could not be observed based on the conventional methods, were obtained with the use of MCR-ALS. As shown in Fig. 3D, a slight red shift was occurred in the absorption spectra of HSA-CAP complex compared to HSA and a major red shift was observed for the HSA$[CAP]_3$ complex compared to HSA. The red shift indicated that the microenvironment of tryptophan residues on HSA has been altered so that the polarity around the Tyr and Trp residues was decreased and the hydrophobicity was decreased [59].

3.6. Molecular docking studies

Molecular docking studies provide some insights into the interaction between small molecule and bio macromolecule [22]. In this paper, to complement our experimental observations and investigate the interaction between CAP and various amino acid residues of HSA in the binding site, molecular docking technology was performed. At first in order to understand the binding mode of CAP on site I and II of HSA, molecular docking was conducted on both sites. As shown in Table 2, the value of $\Delta G_{binding}$ obtained on sites I and II were −6.081 and −5.460 kcal/mol, respectively, which revealed the relatively higher prevalence of CAP toward site I. This is consistent with the results obtained from spectroscopy section and displacement studies reported by Wu and co-workers [19]. Moreover, the obtained value of $\Delta G_{binding}$ from the thermodynamic analysis is $-23.30\,kJ\,mol^{-1}$ or −5.565 kcal/mol, which is in good agreement with Docking results. As can be seen in the docking pose of CAP (Fig. 4A), the binding pocket of CAP in site I was predominantly surrounded by hydrophobic residues, including Arg257, Ser192, Leu238, Glu153, Tyr150, leu219, Leu234, Ser287, Ile290, Leu260, and Ile264. In addition, the Gln196, Lys199, His242, Ala291 residues formed seven hydrogen bonds with CAP. The carbonyl group of Gln196 built two hydrogen bonds with OH groups of CAP with bond lengths of 2.80 and 2.92 Å and energies of −2.30 and −2.40 kcal, respectively. The NH_2 group of the Lys199 side chain formed two hydrogen bonds with hydroxyl and carbonyl group of CAP with bond lengths and energies of 3.03 Å, −7.50 kcal and 3.36 Å, −9.60 kcal, respectively. The NH group of His242 was connected to the carbonyl

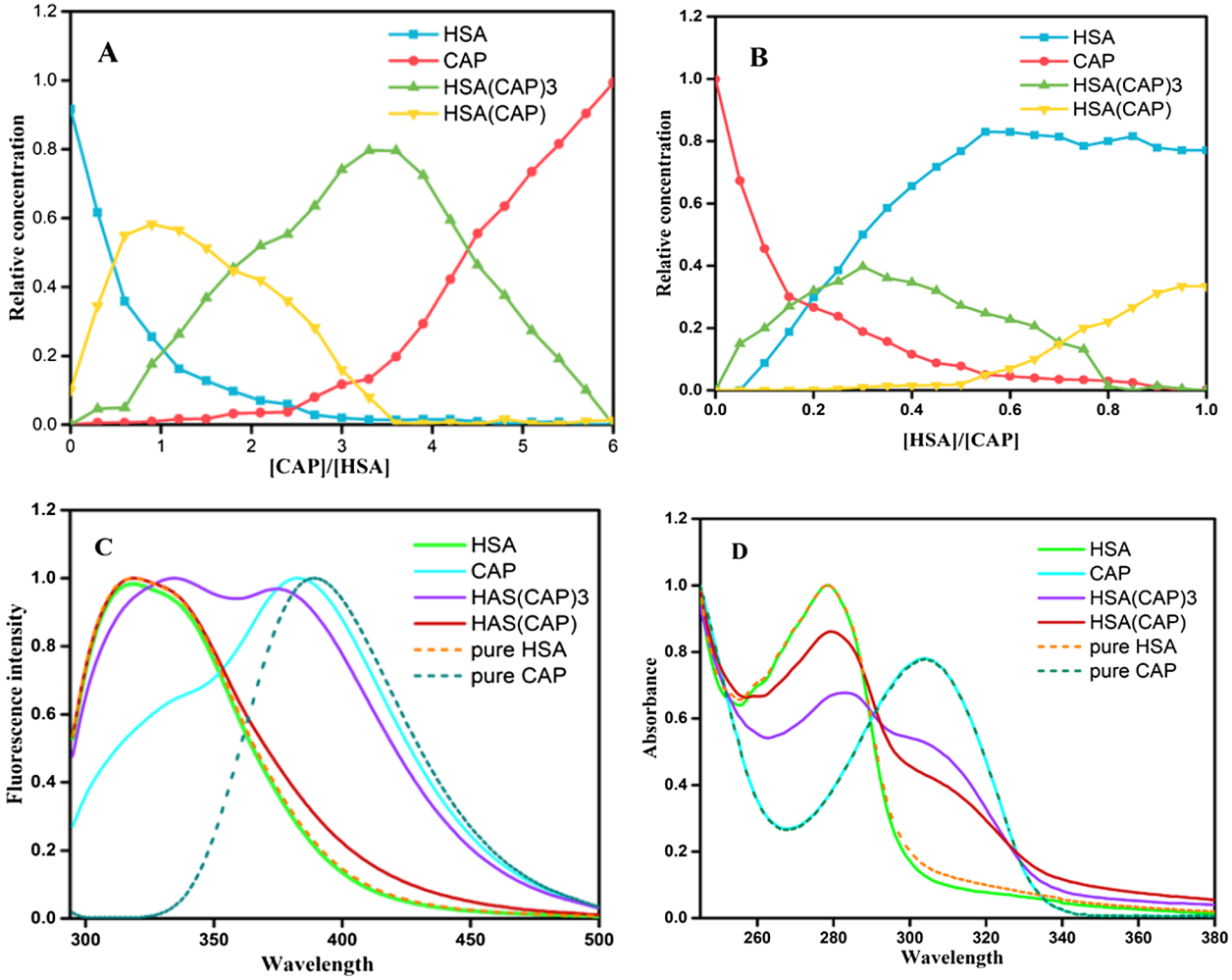

Fig. 3. The results of applying MCR-ALS to augmented matrix: (A) and (B) Extracted concentration profiles of species involved. (C) and (D) Extracted spectral profiles of different species involved in fluorescence and UV–Vis experiment, respectively.

group CAP along with bond lengths and energies of 3.08 Å, −0.90 kcal, respectively. Furthermore, the NH_2 group of Ala291 formed hydrogen bond with carbonyl group of CAP with bond lengths and energies of 3.2 Å, −0.90 kcal, respectively. The obtained molecular docking results indicated that hydrophobic forces as well as hydrogen bonding play a major role in the binding of CAP with HSA, which were consistent with our experimental results.

3.7. Molecular dynamics simulation

MD simulations of 15 ns were performed to provide structural and dynamic information on the interaction between HSA and CAP. Root-mean-square deviation (RMSD), which is a crucial parameter in evaluating the stability of the complex during simulation time, was computed for backbone atoms with respect to the starting structure. The attained RMSD plot of HSA-CAP and HSA as a reference (Fig. 5A) shows that the RMSD value was increased sharply until approximately 2 ns, and then was remained constant until the end of the simulation. This phenomenon indicates that the HSA-CAP complex was relatively stable after 2 ns, so it is reasonable to investigate the binding site based on the snapshots which have been extracted from 2 to 15 ns. The analysis of root mean square fluctuations (RMSFs) of the backbone atoms of HSA in the absence and presence of CAP can be used to reveal a local change in the mobility of residue during the interaction (Fig. 5B). As can be seen in Fig. 5A, the main fluctuations (> 0.35 nm) belong to residues that were far from the ligand binding pocket. In contrast, the residues such as Lys199, Hse242, Arg257, Leu238, etc. that were located in the binding site I of HSA were the most stable residues of this protein (RMSF < 0.10 nm) that involved in the drug contacting. As previously expressed, the CAP-HSA complex was stabilized after 2 ns due to conformational rearrangement, therefore, to further analyze the binding mode during the simulation, average

Table 2
The binding energy, residues involved in H-bond and hydrophobic interactions of HSA–CAP complex in both site I and II.

HSA-CAP complex	Binding energy (kcal Mol^{-1})	Hydrogen bonds interaction	Hydrophobic Interactions
Site I	−6.081	Gln196, Lys199, His242, Ala291	Arg257, Ser192, Leu238, Glu153, Tyr150, leu219, Leu234, Ser287, Ile290, Leu260, Ile264
Site II	−5.460	Ser489, Lys414, Tyr411,	Arg485, Arg410, Leu407, Leu430, Phe403, Val433, Leu453, Asn391, Ala449, Leu387, Ile388, Cys437, Cys438

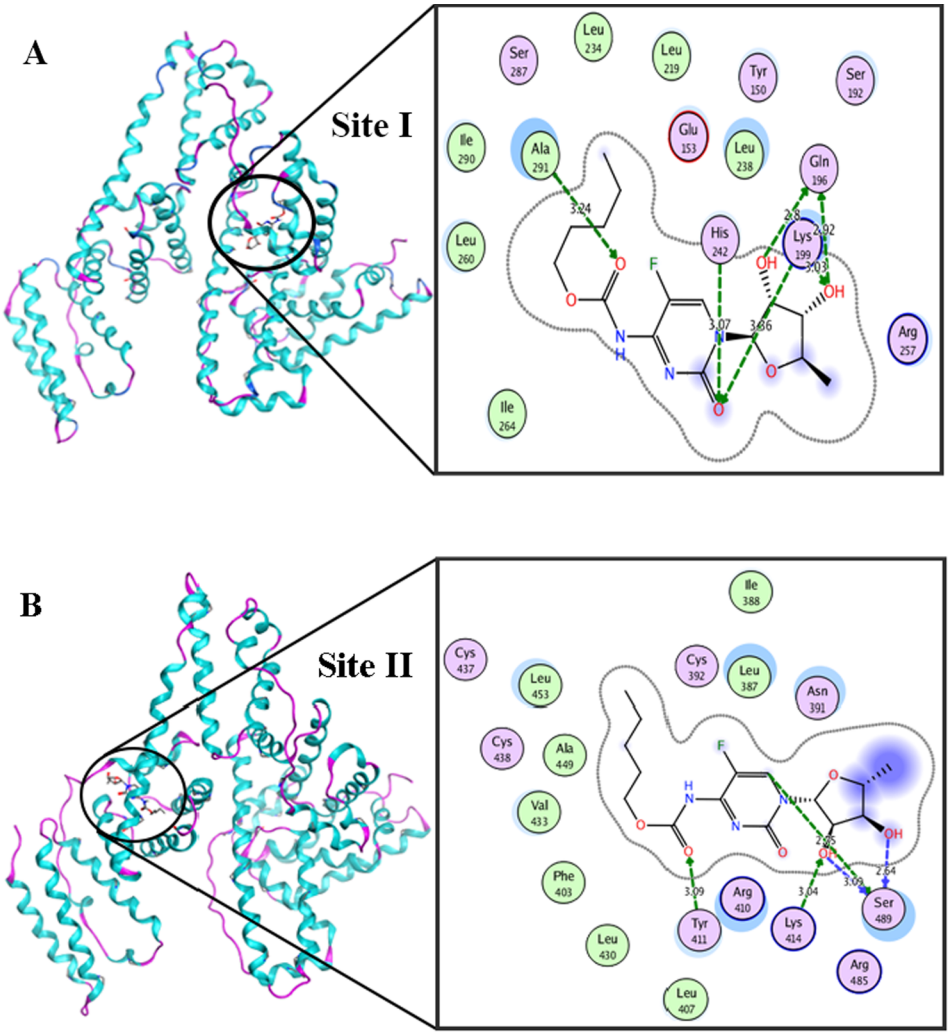

Fig. 4. Binding mode of CAP in the (A) site I and (B) site II of HSA. Residues involved in H-bond are shown as dashed line.

conformation of the binding pocket of HSA complexed with CAP was obtained from the last 100 conformations in the last 3 ns of the MD simulation. As can be seen in Fig. 6, the most key residues have been appeared around the CAP in the binding pocket on the basis of average MD-simulated complex structure are very similar to the results obtained from docking however, several new hydrogen bonds appeared that were not observed in the docking study. Analysis of MD result shows that hydrogen bonds between NH_2 group of the Lys199 and the carbonyl group of CAP, and NH group of His242 and the carbonyl group of CAP, were remained stable throughout the simulation, which indicates that these hydrogen bond interactions were strong. Moreover, a new hydrogen bond was formed between the carboxyl group of Glu153 and hydroxyl group of CAP with bond lengths and energies of 3.2 Å and −0.90 kcal, respectively. The NH group of His242 formed a hydrogen bond with nitrogen groups of CAP with bond lengths and energies of 3.21 Å and −0.90 kcal, respectively. In addition, NH and NH_2 groups of Arg257 could form two hydrogen bonds with carbonyl group of CAP with bond lengths of 3.04 and 2.93 Å and energies of −1.80 and −5.80 kcal, respectively. In addition, phenyl ring of Tyr150 displayed a π-π stacking with cytidine ring of CAP, where, this attractive hydrophobic interaction played an important role in stabilization of CAP in the binding pocket. As a result, the difference between binding mode of CAP after the molecular docking and after the MD can be attributed to the small size of the CAP and the sufficient free space around it in the binding site.

3.8. Fluorescence resonance energy transfer studies

Fluorescence resonance energy transfer (FRET) is a distance-dependent photophysical process in which the energy is transferred from an excited donor fluorophore (HSA) to an acceptor fluorophore (CAP) through the radiationless process [60]. The efficiency of energy transfer depends on the extent of overlap between emission spectrum of donor and absorption spectrum of acceptor, proper dipole orientation of two fluorophore (donor and acceptor), and the distances between donor and acceptor which should be within the forster distance of 2–8 nm [61]. The efficiency of energy transfer (E) can be explained and determined according to the forster energy transfer theory by using the following equation:

$$E = 1 - \frac{F}{F_0} = \frac{R_0^6}{R_0^6 + r^6} \quad (8)$$

Here, F and F_0 are fluorescence intensities of the donor (HSA) in the presence and absence of the acceptor (CAP), r is the distance from the acceptor (CAP) to tryptophan residue of (HSA), and R_0 is the forster critical distance, when the transfer efficiency is 50%, which can be calculated by Eq. (9):

$$R_0^6 = 8.79 \times 10^{-25} K^2 n^{-4} \varnothing J \quad (9)$$

where, K is the spatial orientation factor related to the geometry of the

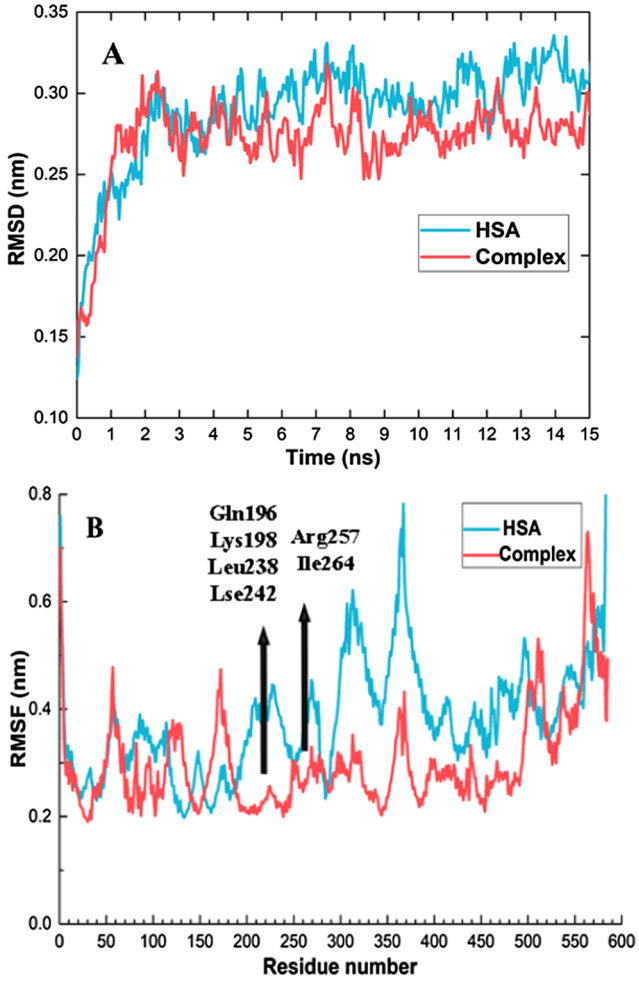

Fig. 5. (A) The root mean square deviations (RMSD) versus the MD simulation time for HSA (blue) and HSA-CAP complex (red) in the MD simulation system. (b) RMSF value of each residue of HSA during the entire simulation time, in absence and presence of CAP. (For interpretation of the references to colour in this figure legend, the reader is referred to the web version of this article.)

donor and acceptor, n is the refractive index of the medium surrounding the fluorophores, ∅ is the fluorescence quantum yield of the donor in the absence of an acceptor, and J is the overlap integral of the fluorescence emission spectrum for the donor and the absorption spectrum of the acceptor (Fig. S2), which could be calculated by the following equation:

$$J = \frac{\int_0^\infty F(\lambda)\varepsilon(\lambda)\lambda^4(d\lambda)}{\int_0^\infty F(\lambda)\mathrm{d}\lambda} \quad (10)$$

where F(λ) and ε(λ) are the fluorescence intensity of the HSA and molar absorption coefficient of the CAP at wavelength λ, respectively.

The overlap between the absorption spectrum of CAP and the fluorescence emission spectrum of HSA is shown in Fig. S2. The values of K^2, *n*, and ∅ for HSA–ligand bindings are reported as 2/3, 1.336 and 0.118, respectively [62]. Thus, according to the above equations the values of J, R_0, E and *r* were calculated to be 1.16×10^{-13} cm^3 L mol^{-1}, 3.92 nm, 0.41 and 4.135 nm, respectively. Meanwhile, the average distance between CAP and Trp residues of HSA was far less than 8 nm and $0.5R_0 < r < 1.5\ R_0$ which indicated that the energy transfer from Trp of HSA to CAP occurs with high probability. Furthermore, the larger value of r in comparison to R_0 revealed the presence of static type quenching mechanism for the interaction of CAP with HSA [63,64].

4. Conclusion

In the current study, the interaction of CAP with HSA was investigated by fluorescence and UV–Vis spectroscopies. These procedures were combined with molecular modeling method to further analyze the HSA-CAP system under simulated physiological conditions. According to fluorescence emission spectra, the fluorescence intensity of HSA was gradually decreased and a new intensive peak was appeared at 387 nm upon the addition of CAP, which indicates the formation of a complex between CAP and HSA. Moreover, UV–Vis results showed that the binding of CAP to HSA leads to changes in the protein secondary structure. Based on the fluorescence quenching studies, it can be stated that CAP quench the inherent fluorescence intensity of HSA via the static quenching rather than dynamic quenching. The values of binding constant were determined which showed a moderate binding affinity between CAP and HSA and the efficiency of energy transfer was obtained to be 0.41. The obtained thermodynamic parameters revealed that hydrogen bonds and van der Waals forces played a major role in stabilizing the CAP–HSA complex. The resolved concentration profiles by MCR-ALS revealed that in addition to pure signals for HSA and CAP, there were two other complex species with a ratio of 1:1 and 1:3. The results derived from molecular docking exhibited that the CAP had higher prevalence toward site I which coincided well with the

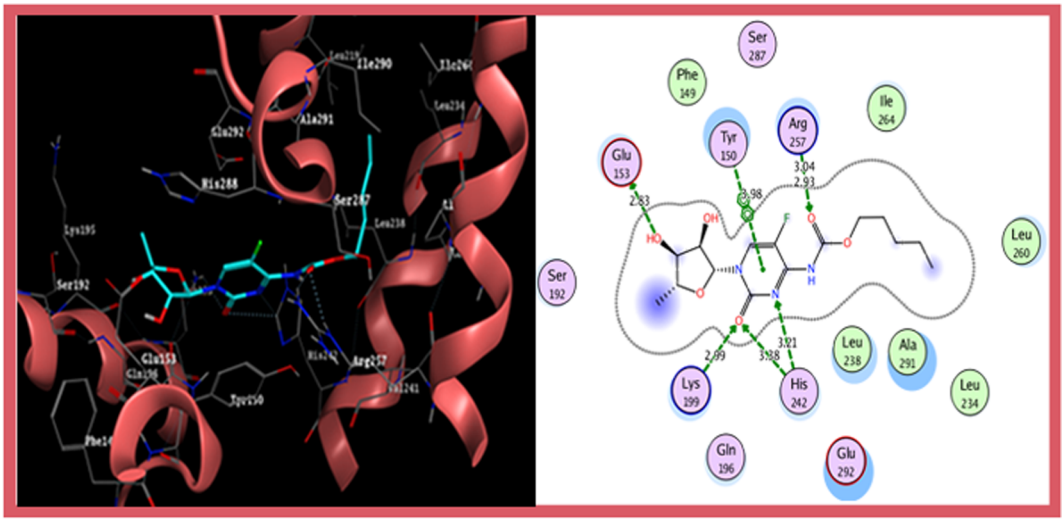

Fig. 6. Plot of the MD-simulated structures of capecitabine in the binding site of HSA.

experimental results. Moreover, MD results showed that the HSA and HSA-CAP complex achieved stability after about 2 ns. Analysis of CAP binding mode after MD showed different interaction between CAP and HSA residues compared with docking binding mode which can be attributed to the small size of the CAP and the sufficient free space around it in the binding site. Finally, the present study provides insights into the binding mechanism of CAP and HSA which can facilitate further investigations on pharmacological properties of CAP.

Appendix A. Supplementary material

Supplementary data to this article can be found online at https://doi.org/10.1016/j.bioorg.2019.103037.

References

[1] J.L. Grem, 5-Fluorouracil: forty-plus and still ticking. A review of its preclinical and clinical development, Invest. New Drugs 18 (2000) 299–313.
[2] R.J. Rutman, A. Cantarow, K.E. Paschkis, Studies in 2-acetylaminofluorene carcinogenesis: III. The utilization of uracil-2-C14 by preneoplastic rat liver and rat hepatoma, Cancer Res. 14 (1954) 119–123.
[3] R.M. Wohlhueter, R.S. McIvor, P.G. Plagemann, Facilitated transport of uracil and 5-fluorouracil, and permeation of orotic acid into cultured mammalian cells, J. Cell. Physiol 104 (1980) 309–319.
[4] A.J. Wagstaff, T. Ibbotson, K.L. Goa, Capecitabine, Drugs 63 (2003) 217–236.
[5] M. Miwa, M. Ura, M. Nishida, N. Sawada, T. Ishikawa, K. Mori, N. Shimma, I. Umeda, H. Ishitsuka, Design of a novel oral fluoropyrimidine carbamate, capecitabine, which generates 5-fluorouracil selectively in tumours by enzymes concentrated in human liver and cancer tissue, Eur J. Cancer 34 (1998) 1274–1281.
[6] D. Garg, S. Henrich, O.M. Salo-Ahen, H. Myllykallio, M.P. Costi, R.C. Wade, Novel approaches for targeting thymidylate synthase to overcome the resistance and toxicity of anticancer drugs, J. Med. Chem. 53 (2010) 6539–6549.
[7] C. Bertucci, E. Domenici, Reversible and covalent binding of drugs to human serum albumin: methodological approaches and physiological relevance, Curr. Med. Chem 9 (2002) 1463–1481.
[8] U. Kragh-Hansen, Molecular aspects of ligand binding to serum albumin, Pharmacol Rev 33 (1981) 17–53.
[9] A.M. Talbert, G.E. Tranter, E. Holmes, P.L. Francis, Determination of drug-plasma protein binding kinetics and equilibria by chromatographic profiling: Exemplification of the method using l-tryptophan and albumin, Anal. Chem. 74 (2002) 446–452.
[10] X.M. He, D.C. Carter, Atomic structure and chemistry of human serum albumin, Nature 358 (1992) 209.
[11] G. Sudlow, D. Birkett, D. Wade, Further characterization of specific drug binding sites on human serum albumin, Mol. Pharmacol. 12 (1976) 1052–1061.
[12] S. Curry, H. Mandelkow, P. Brick, N. Franks, Crystal structure of human serum albumin complexed with fatty acid reveals an asymmetric distribution of binding sites, Nat. Struct. Mol. Biol. 5 (1998) 827.
[13] T.A. Wani, A.H. Bakheit, M.N. Ansari, A.-R.A. Al-Majed, B.M. Al-Qahtani, S. Zargar, Spectroscopic and molecular modeling studies of binding interaction between bovine serum albumin and roflumilast, Drug Des. Dev. Ther. 12 (2018) 2627.
[14] T.A. Wani, H. AlRabiah, A.H. Bakheit, M.A. Kalam, S. Zargar, Study of binding interaction of rivaroxaban with bovine serum albumin using multi-spectroscopic and molecular docking approach, Chem. Cent. J. 11 (2017) 134.
[15] T.A. Wani, A.H. Bakheit, S. Zargar, M.A. Hamidaddin, I.A. Darwish, Spectrophotometric and molecular modelling studies on in vitro interaction of tyrosine kinase inhibitor linifanib with bovine serum albumin, PloS One 12 (2017) e0176015.
[16] T. Wani, A. Bakheit, A.-R. Al-Majed, M. Bhat, S. Zargar, Study of the interactions of bovine serum albumin with the new anti-inflammatory agent 4-(1, 3-Dioxo-1, 3-dihydro-2H-isoindol-2-yl)-N′-[(4-ethoxy-phenyl) methylidene] benzohydrazide using a multi-spectroscopic approach and molecular docking, Molecules 22 (2017) 1258.
[17] S. Abbasi, A. Benvidi, S. Gharaghani, M. Rezaeinasab, Chemometric studies of thymol binding with bovine serum albumin: A developing strategy for the successful investigation of pharmacological activity, Bioelectrochemistry 124 (2018) 172–184.
[18] M. Salary, M. Hadjmohammadi, Human serum albumin-mimetic chromatography based hexadecyltrimethylammonium bromide as a novel direct probe for protein binding of acidic drugs, J. Pharm. Biomed. Anal. 114 (2015) 1–7.
[19] D. Wu, J. Yan, P. Sun, K. Xu, S. Li, H. Yang, H. Li, Comparative analysis of the interaction of capecitabine and gefitinib with human serum albumin using 19F nuclear magnetic resonance-based approach, J. Pharm. Biomed. Anal. 129 (2016) 15–20.
[20] N.S. Jha, N. Kishore, Thermodynamic studies on the interaction of folic acid with bovine serum albumin, J. Chem. Thermodyn. 43 (2011) 814–821.
[21] R. De-Llanos, S. Sánchez-Cortes, C. Domingo, J.V. García-Ramos, P. Sevilla, Surface plasmon effects on the binding of antitumoral drug emodin to bovine serum albumin, J. Phys. Chem. C 115 (2011) 12419–12429.
[22] S.F. Mousavi, M.H. Fatemi, A combination of molecular docking, receptor-guided QSAR, and molecular dynamics simulation studies of S-trityl-l-cysteine analogues as kinesin Eg5 inhibitors, Struct. Chem. 30 (2019) 115–126.
[23] G. Mohammadi, E. Faramarzi, M. Mahmoudi, S. Ghobadi, A.R. Ghiasvand, H.C. Goicoechea, A.R. Jalalvand, Chemometrics-assisted investigation of interactions of Tasmar with human serum albumin at a glassy carbon disk: Application to electrochemical biosensing of electro-inactive serum albumin, J. Pharm. Biomed. Anal. 156 (2018) 23–35.
[24] M. Frisch, G. Trucks, H.B. Schlegel, G.E. Scuseria, M.A. Robb, J.R. Cheeseman, G. Scalmani, V. Barone, B. Mennucci, G. Petersson, Gaussian 09, revision a. 02, gaussian, Inc., Wallingford, CT, 200, 2009.
[25] J. Ghuman, P.A. Zunszain, I. Petitpas, A.A. Bhattacharya, M. Otagiri, S. Curry, Structural basis of the drug-binding specificity of human serum albumin, J. Mol. Biol. Mol. 353 (2005) 38–52.
[26] G.M. Morris, R. Huey, W. Lindstrom, M.F. Sanner, R.K. Belew, D.S. Goodsell, A.J. Olson, AutoDock4 and AutoDockTools4: Automated docking with selective receptor flexibility, J. Comput. Chem. 30 (2009) 2785–2791.
[27] J.C. Phillips, R. Braun, W. Wang, J. Gumbart, E. Tajkhorshid, E. Villa, C. Chipot, R.D. Skeel, L. Kale, K. Schulten, Scalable molecular dynamics with NAMD, J. Comput. Chem. 26 (2005) 1781–1802.
[28] J. Jaumot, R. Gargallo, A. de Juan, R. Tauler, A graphical user-friendly interface for MCR-ALS: a new tool for multivariate curve resolution in MATLAB, Chemom. Intell. Lab. Syst. 76 (2005) 101–110.
[29] T. Azzouz, R. Tauler, Application of multivariate curve resolution alternating least squares (MCR-ALS) to the quantitative analysis of pharmaceutical and agricultural samples, Talanta 74 (2008) 1201–1210.
[30] M. Vives, R. Gargallo, R. Tauler, Study of the intercalation equilibrium between the polynucleotide poly (adenylic)– poly (uridylic) acid and the ethidium bromide dye by means of multivariate curve resolution and the multivariate extension of the continuous variation and mole ratio methods, Anal. Chem. 71 (1999) 4328–4337.
[31] A. de Juan, J. Jaumot, R. Tauler, Multivariate Curve Resolution (MCR). Solving the mixture analysis problem, Anal. Methods 6 (2014) 4964–4976.
[32] F. Azimi, M.H. Fatemi, Multivariate curve resolution-correlation optimized warping applied to the complex GC-MS signals; toward comparative study of peel chemical variability of Citrus aurantium L. varieties, Microchem. J. 143 (2018) 99–109.
[33] M. De Luca, G. Ragno, G. Ioele, R. Tauler, Multivariate curve resolution of incomplete fused multiset data from chromatographic and spectrophotometric analyses for drug photostability studies, Anal. Chim. Acta 837 (2014) 31–37.
[34] C. Ruckebusch, L. Blanchet, Multivariate curve resolution: a review of advanced and tailored applications and challenges, Anal. Chim. Acta 765 (2013) 28–36.
[35] J. Jaumot, A. de Juan, R. Tauler, MCR-ALS GUI 2.0: new features and applications, Chemom. Intell. Lab. Syst. 140 (2015) 1–12.
[36] A. Fiser, R.K.G. Do, Modeling of loops in protein structures, Protein Sci. 9 (2000) 1753–1773.
[37] V. Zoete, M.A. Cuendet, A. Grosdidier, O. Michielin, SwissParam: a fast force field generation tool for small organic molecules, J. Comput. Chem. 32 (2011) 2359–2368.
[38] J.-P. Ryckaert, G. Ciccotti, H.J. Berendsen, Numerical integration of the cartesian equations of motion of a system with constraints: molecular dynamics of n-alkanes, J. Comput. Phys. 23 (1977) 327–341.
[39] T. Darden, D. York, L. Pedersen, Particle mesh Ewald: An N· log (N) method for Ewald sums in large systems, J. Comput. Phys. 98 (1993) 10089–10092.
[40] J. He, D. Wu, Y. Zhai, Q. Wang, X. Ma, H. Yang, H. Li, Interaction of inosine with human serum albumin as determined by NMR relaxation data and fluorescence methodology, J. Mol. Liq. 219 (2016) 547–553.
[41] G.-F. Zhu, Y. Wang, L. Xi, J. Liu, H. Wang, L.-F. Du, Spectroscopy and molecular docking studies on the binding of propyl gallate to human serum albumin, J. Lumin 159 (2015) 188–196.
[42] S. Ashoka, J. Seetharamappa, P. Kandagal, S. Shaikh, Investigation of the interaction between trazodone hydrochloride and bovine serum albumin, J. Lumin 121 (2006) 179–186.
[43] S. Sarzehi, J. Chamani, Investigation on the interaction between tamoxifen and human holo-transferrin: determination of the binding mechanism by fluorescence quenching, resonance light scattering and circular dichroism methods, Int. J. Biol. Macromol. 47 (2010) 558–569.
[44] B.J. Boersma, T. D'Alessandro, M.R. Benton, M. Kirk, L.S. Wilson, J. Prasain, N.P. Botting, S. Barnes, V.M. Darley-Usmar, R.P. Patel, Neutrophil myeloperoxidase chlorinates and nitrates soy isoflavones and enhances their antioxidant properties, Free Radic Biol. Med. 35 (2003) 1417–1430.
[45] M.R. Eftink, Fluorescence Quenching: Theory and Applications, Topics in Fluorescence Spectroscopy, Springer, 2002, pp. 53–126.
[46] M.R. Eftink, C.A. Ghiron, Fluorescence quenching studies with proteins, Anal. Biochem. 114 (1981) 199–227.
[47] M.R. Ajmal, N. Zaidi, P. Alam, S. Nusrat, M.K. Siddiqi, G. Badr, M.H. Mahmoud, R.H. Khan, Insight into the Interaction of antitubercular and anticancer compound Clofazimine with Human Serum Albumin: spectroscopy and molecular modelling, J. Biomol. Struct. Dyn. 35 (2017) 46–57.
[48] Y.-J. Hu, Y. Ou-Yang, C.-M. Dai, Y. Liu, X.-H. Xiao, Site-selective binding of human serum albumin by palmatine: spectroscopic approach, Biomacromolecules 11 (2009) 106–112.
[49] G. Colmenarejo, A. Alvarez-Pedraglio, J.-L. Lavandera, Cheminformatic models to predict binding affinities to human serum albumin, J. Med. Chem. 44 (2001) 4370–4378.
[50] J. Zhang, X.-J. Wang, Y.-J. Yan, W.-S. Xiang, Comparative studies on the interaction of genistein, 8-chlorogenistein, and 3′, 8-dichlorogenistein with bovine serum albumin, J. Agric. Food Chem. 59 (2011) 7506–7513.
[51] J. Xiao, M. Suzuki, X. Jiang, X. Chen, K. Yamamoto, F. Ren, M. Xu, Influence of B-ring hydroxylation on interactions of flavonols with bovine serum albumin, J.

Agric. Food Chem. 56 (2008) 2350–2356.
[52] H.-M. Zhang, Z.-H. Fei, B.-P. Tang, J. Chen, W.-H. Tao, Y.-Q. Wang, The interaction of blood proteins with brucine, Mol. Biol. Rep. 39 (2012) 4937–4947.
[53] F. Pasban Ziyarat, A. Asoodeh, Z. Sharif Barfeh, M. Pirouzi, J. Chamani, Probing the interaction of lysozyme with ciprofloxacin in the presence of different-sized Ag nano-particles by multispectroscopic techniques and isothermal titration calorimetry, J. Biomol. Struct. Dyn. 32 (2014) 613–629.
[54] L. Xu, Y.-X. Hu, J. Li, Y.-F. Liu, L. Zhang, H.-X. Ai, H.-S. Liu, Probing the binding reaction of cytarabine to human serum albumin using multispectroscopic techniques with the aid of molecular docking, J. Photochem. Photobiol. 173 (2017) 187–195.
[55] S. Tabassum, M. Ahmad, M. Afzal, M. Zaki, P.K. Bharadwaj, Synthesis and structure elucidation of a copper (II) Schiff-base complex: in vitro DNA binding, pBR322 plasmid cleavage and HSA binding studies, J. Photochem. Photobiol. 140 (2014) 321–331.
[56] P.D. Ross, S. Subramanian, Thermodynamics of protein association reactions: forces contributing to stability, Biochemistry 20 (1981) 3096–3102.
[57] Z. Chi, R. Liu, H. Zhang, Noncovalent interaction of oxytetracycline with the enzyme trypsin, Biomacromolecules 11 (2010) 2454–2459.
[58] B. Ojha, G. Das, The interaction of 5-(alkoxy) naphthalen-1-amine with bovine serum albumin and its effect on the conformation of protein, J. Phys. Chem. B 114 (2010) 3979–3986.
[59] L. Stryer, Fluorescence spectroscopy of proteins, Science 162 (1968) 526–533.
[60] H. Xu, N. Yao, H. Xu, T. Wang, G. Li, Z. Li, Characterization of the interaction between eupatorin and bovine serum albumin by spectroscopic and molecular modeling methods, Int. J. Mol. Sci. 14 (2013) 14185–14203.
[61] B. Valeur, J.-C. Brochon, New Trends in Fluorescence Spectroscopy: Applications to Chemical and Life Sciences, Springer Science & Business Media, 2012.
[62] D.E. Epps, T.J. Raub, V. Caiolfa, A. Chiari, M. Zamai, Determination of the affinity of drugs toward serum albumin by measurement of the quenching of the intrinsic tryptophan fluorescence of the protein, J. Pharm. Pharmacol. 51 (1999) 41–48.
[63] J. Pan, Z. Ye, X. Cai, L. Wang, Z. Cao, Biophysical study on the interaction of ceftriaxone sodium with bovine serum albumin using spectroscopic methods, J. Biochem. Mol. Toxic 26 (2012) 487–492.
[64] F. Manouchehri, Y. Izadmanesh, E. Aghaee, J.B. Ghasemi, Experimental, computational and chemometrics studies of BSA-vitamin B6 interaction by UV–Vis, FT-IR, fluorescence spectroscopy, molecular dynamics simulation and hard-soft modeling methods, Bioorg. Chem. 68 (2016) 124–136.